

Field-assisted self-assembly at fluid-fluid interfaces

¹*Priyanka Biswas,²Gaurav Pransu

¹Department of Science, Alliance University, Bengaluru 562106, India

²Institute of Physics, Bijenička cesta 46, 10000 Zagreb, Croatia

* priyanka.biswas@alliance.edu.in

Abstract. Self-assembly of particles at fluid-fluid interfaces is a ubiquitous phenomenon. Over the years scientists have tried to modulate and direct self-assembly processes using various intrinsic and extrinsic parameters. This review article presents the situation where self-assembly of mesoscopic particles at interfaces is controlled by external fields, namely, electric, and magnetic fields. By controlling the shape and size of the particles, the attractive forces can be tuned. Moreover, strength and direction of external fields also play important roles in deciding the final assembled structure. These systems hold great potential in novel designs for drug delivery, catalysis and other transport phenomena.

Keywords. self-assembly; fluid interfaces; nanoparticles.

1 Introduction

Over the years, self-assembly has become one of the most used term in field of soft matter science. It is defined as the spontaneous organization of units (molecules, colloids, micelles, etc.) forming ordered structures without the direct influence of any external forces. This is the precise reason why there is so much curiosity in this field as self-assembly is energy efficient and could occur in multiple steps ensuring a facile “bottom-up” approach in manufacturing novel functional materials.[1] The concept is essentially rooted in the evolution of life from unicellular organisms. With the advent of technological advancements, this method have been mimicked in multiple fields aimed at building hierarchical structures from micro-or nanoscale units fulfilling a specific function for application-based uses in field of electronics,[2,] photonics[3], memory devices,[4] etc. Focusing on colloidal chemistry specifically, enormous amount of literature has flourished over the last decades on the topic of colloidal self-assembly.[5]From a fundamental point of view, the study of intrinsic factors governing the self-assembly of particles is crucial to obtain the desired structure and functionality of the nano-structured device. Interparticle interactions include electro- static, van der Waals forces, etc. whereas extrinsic factors comprises of external fields, capillarity, etc.[6] These interactions depend on various factors such as shape, size, surface charge, etc. The energetics involved in the particle interactions compare with the thermal energy of the surrounding medium which makes it feasible for the system to autonomously explore the energy landscape until it eventually reaches the ground state configuration.

With the availability of an external field, the scenario alters. Various field-assisted assembly techniques have emerged which are aimed to provide better external control on the assembly process resulting in precision and desired hierarchy in terms of engineering. Nonetheless, the self-assembled structures formed under specific conditions are some of the low energy configurations. Trapping of nanoparticles at fluid-fluid interfaces is one of the oldest and most promising techniques to in- duce ordering in a colloidal system. Particles remain irreversibly trapped, as the interfacial energy is lowered at this configuration. The implications of such behaviour are perceived by the ability of nanoparticles to stabilize emulsions and foams. A classic example of this dates back to almost a century ago when Ramsden[7] and Pickering[8] investigated the stability of paraffin-water emulsions by micrometric-sized colloidal particles of silica, iron oxide, kaolin etc. The colloidal particle got trapped at the interface, lowering the interfacial tension and leading to 2D assemblies resembling colloidal crystals. These emulsions were consequently named after Pickering. Long after that, Pieranski[9], investigated particle-particle interaction for polystyrene (PS) at an air-water interface. Asymmetry of charge distribution at the interface causes the particles to behave as electrical dipoles. The dipole-dipole repulsive interactions organize the polystyrene spheres into a 2D triangular lattice because of the decrease in the total free energy. The energy required to desorb a particle depends on the particle size, shape and the interparticle interactions along with interface-particle interactions. Interesting observations followed thereafter when it was found that stabilization of nanoparticles was more difficult energetically, as the order of their desorption energies compared with the order of thermal energy. Hence they are easily displaced leading to particle exchange at the interface.

One of the ways to lock-in these particles into desired arrangements is by external fields if they are receptive to them, such as magnetic nanoparticles by an external magnetic field, charged particles by an electric field, thermal gradient, etc.[10] The confinement and symmetry-breaking at the interface play a crucial role in regulating the response of the particles to the external field. The responsiveness of the particles to the external field is again significantly dependent on surface charges, shape, and sizes. This review

is concerned with the status of research on field-assisted self-assembly of particles at fluid interfaces. The article gives both a unified overview of recent experimental advances and theoretical studies in this regard, starting with discussing the cases for single particles (both spherical and non-spherical shapes) followed by interparticle interactions at interfaces. The possibility of remotely controlling and manipulating particle assembly without perturbing the surrounding medium, together with strong confinement induced by the adsorption at the boundary, makes interfaces excellent model systems to realize application-based functional nano-machinery.

2 ISOLATED PARTICLES AT FLUID-FLUID INTERFACE

To understand the behaviour of trapped particles at the interface, we start with an isolated particle. It is important to understand the consequence of single particle adsorption on the interface to generalize the case into a group of particles and subsequently to assess the extent of influence of an external field. Consider a particle in suspension near a planar fluid-fluid interface. When the particle attaches to the interface, it eliminates a patch of fluid-fluid contact ΔA_{P1} corresponding to the area displaced by the particle from fluid 1 making a hole in the interface of the fluids of area ΔA_{12} . Furthermore, it can make distortions in the surrounding interface with area δA . The net energy change or trapping energy ΔE at the interface is given by

$$\Delta E = (\gamma_{P1} - \gamma_{P2}) \cdot A_{P1} + \gamma_{12} \Delta A_{12} + \gamma_{12} \delta A \quad (1)$$

where γ_{P1} and γ_{P2} are the surface energies per unit area of the particle-fluid 1 and particle-fluid 2 surfaces, γ_{12} is the surface tension between fluid 1 and 2. The difference in free energy between the two states (before and after particle trapping) determines the preferred particle orientation in the case of physically anisotropic particles where there can be multiple orientations. This can be considered as a thumb rule to predict the orientation of ellipsoids, dumb-bells[11] and other anisotropic geometries as well. Some well-known anisotropic particles include disks[12], cubes[13] in addition to the special case of Janus, or patchy particles which have two or more chemically or physically dissimilar regions[14]. When the trapping energy is large compared with $k_B T$, the particle is trapped; i.e., it cannot spontaneously leave the interface. Trapping particles at fluid-fluid interfaces is a very robust way to carry out nanoparticle assembly. The dominant driving force for getting the particles to assemble at the interface is the reduction in interfacial energy, and the assembly is further controlled by lateral interface-mediated capillary forces. Now we investigate the case of spherical particles, which is the simplest type of symmetry. Needless to mention the complexity of the energy expression increases as the symmetry folds decrease, as we shall cover in a later section.

2.1 Spherical particle

As mentioned earlier, Pieranski [9] in 1980 drew attention to the system of spherical PS particles forming crystal-like ordering at flat interfaces. To have a clearer picture of the underlying forces driving the assembly, we focus on one spherical particle of radius r resting at a flat interface between fluid 1 and fluid 2. Let θ_c be the contact angle (Fig 1). The particle can attach without deforming the surrounding interface, so $\delta A = 0$, and the contact line is simply a circle in the plane of the interface. Neglecting any other external forces and a finite thickness of the interface, the net trapping energy is

$$\Delta E = -\gamma_{12} \pi r^2 (1 - |\cos \theta_c|)^2 \quad (2)$$

Where $\cos(\theta_c) = (\gamma_{P1} - \gamma_{P2}) / \gamma_{12}$.

By attaching, the particle reduces the area of the fluid-fluid interface, lowering the system energy. This effect is modulated by the particle-wetting properties. Perfectly smooth spheres with homogeneous wetting conditions leave the interface around them unperturbed and the trapping energy is remarkably large. However, partial wetting causes interface distortion. For example, for air-water interfaces, the surface tension is $\gamma_{12} = 72 \text{ mN/m}$ or $18 k_B T / \text{nm}^2$. Typical trapping energies for microparticles can be $10^5 - 10^6 k_B T$ compared to thermal energy (a few $k_B T$), leading to strong trapping at the interfaces. Nanoparticles on the other hand have a lower trapping energy of $10 - 10^2 k_B T$. Therefore, thermal randomization can displace nanoparticles from the interfaces more easily than micron-sized particles. Contact-line pinning is another factor that determines the trapping energy and contributes to interface distortion around them. Pinning occurs due to nanoscopic sites of roughness on the particle or chemical heterogeneity due to which the contact lines distort the interface around them, so in Eq. 1, $\delta A \neq 0$. [15] For isolated particles, contact line pinning changes the trapping energy by the amount $\gamma_{12} \delta A$; this is termed a self-energy contribution.[16]. For spherical particles with pinned contact lines, several unknown aspects complicate the evaluation of the trapping energy. These include the unknown

angle characterizing the degree of immersion of the particle in the fluid. In that case, this angle replaces the contact angle in Eq. 2. The "self-energy", δA of Eq. 1 is now the associated area of particle-sourced deformation in the interface. δA can be obtained by decomposing the shape of the contact line into Fourier modes, factoring in the height of the interface around the particle above the reference plane and evaluating the associated area for each mode. Similar terms appear from the higher-order modes in the multipole expansion.

2.2 Non-spherical particle

The most common cases of assembly at the interface have trapped spherical particles. With the momentous advancements in the synthesis of anisotropic-shaped nanoparticles, these have become unique case studies about their behaviour at interfaces. Anisotropic particles have been reported to provide additional control of light propagation for photonic crystals[17] and function as efficient nanocarriers for drug delivery applications.[18] They can also give rise to interesting and unique behavior when dispersed in nematic liquid crystals,[19] and exhibit non-Newtonian rheological properties[20]. A non-spherical particle must distort the interface to maintain a constant contact angle. Thus, the assumption of the fluid interface to be planar does not hold valid in this case. The contributions to the trapping energy remain the same for complex-shaped particles. These include the energy decrease caused by the hole in the interface (ΔA_{12}), modulated by the particle wetting energies, and the energy caused by the excess area of the interface distortion (δA). The evaluation of each contribution is difficult for many reasons. The equilibrium wetting configuration of complex-shaped particles cannot typically be derived analytically.[21,22] Thus, the size of the hole in the interface, the height of the particle, and the interface distortion must typically be found via simulation. However, for visual estimation purposes, the relevant terms are represented in Fig 1. As described in the case of spherical particles, the pinned contact lines around nonspherical particles can also be decomposed into Fourier modes.

For elongated particles, the expansion is carried out in ellipsoidal coordinates for a particular particle aspect ratio. The quadrupolar modes in this coordinate describe the far-field interface shape for elongated particles. An aspect ratio and contact angle phase diagram could be constructed that depicts the end-on or side-on configuration of isolated cylinders.[21] Eq. 3 shows the dependence of the free energy of ellipsoidal particles with the line tension τ . Bresme *et al.* [23] calculated the trapping energy and its dependence on an applied external field. They reported that the most stable configuration in the absence of any external field is the parallel one, since this configuration maximizes the area removed from the fluid-fluid interface. The difference in the free energy of the parallel and perpendicular configurations increases with the aspect ratio. Hence the larger the aspect ratio, the less stable is the perpendicular configuration concerning the parallel one. Bresme calculated the trapping energy for a nanometric particle with an aspect ratio of 2:1 at oil-water interface, this gives a trapping energy of the order of 10^2 and $2 \times 10^2 k_B T$ at ambient temperature for perpendicular and parallel configurations respectively. For an aspect ratio of 10:1, the difference of trapping energy is about $10^3 k_B T$ and thus it is quite unlikely to find particles in the perpendicular orientation. Nonetheless, it is important to note that the free energy difference strongly depends on the interfacial tension. However, for low surface tension interfaces the differences in free energy are dramatically reduced suggesting that an external perturbation, such as a magnetic or electrostatic field, could stabilize the vertical orientation with respect to the horizontal one as will be discussed later. Anisotropically shaped microparticles attach to interfaces via a process similar to that for spheres. Wang *et al.* [24] demonstrated that an ellipsoidal microparticle enters the interface via a rolling motion due to non-uniform displacement of contact line segments. Any complex-shaped particle can assume a variety of configurations.[25, 21] However, it should be noted that any isolated particle, without the influence of external field, assume orientations in which they make the largest hole in the interface; e.g., elongated particles have their long axes in the plane of the interface. In contrast, thin disks or rods with a small aspect ratio typically adsorb at aqueous-oil interfaces with their circular face in the interface.[26] Rod-shaped colloids are one of the most commonly studied systems due to their ease in functionalization to exhibit various optical, electrical, or magnetic properties [27, 28] In bulk, nanorods exhibit liquid crystal-type phase behaviour at certain aspect ratios. Whereas at the interface the orientation also depends on a variety of factors such as aspect ratio, wettability, etc. The general expression for trapping the energy of an isolated ellipsoid or rod-like at a fluid-fluid interface is [29]

$$\Delta E = (\gamma_{P1} - \gamma_{P2}) \cdot A_{P1} - \gamma_{12} \Delta A_{12} + \tau L \quad (3)$$

where τ is the line tension of the three-phase line, and L is the length of the three-phase line. The relevant parameters are depicted in Fig 1. Line tension becomes an important factor for small micrometer-sized and large nanometer-sized particles. Line tension may qualitatively alter the behaviour of non-spherical particles at interfaces causing them to undergo orientational changes to minimize the length of the contact line. Faraudo [29] provided the expression for free energies of ellipsoids in two orientations: one in which the major axis is parallel ($\Delta E_{parallel}$) to the interface plane, and a second one in which it is normal to

the interface (E_{perp}) given by,

$$\Delta E_{parallel} = 2\pi r L [\pi(\gamma_{P1} - \gamma_{P2}) + \theta_c(\gamma_{P2} - \gamma_{P1}) + \gamma_{12} \sin \theta_c] \quad (4)$$

$$\Delta E_{perp} = (\gamma_{P2} - \gamma_{12} - \gamma_{P1})\pi r^2 + (\gamma_{P2} - \gamma_{P1})2\pi r h \quad (5)$$

where r is the cross-sectional radius of the ellipse and h is the penetration depth of the nanorods in the water phase when assembled normally to the interface (Fig. 1). Thus, isolated nanorods orient parallel to the plane of the interface to maximize the interfacial coverage per particle and minimize the Helmholtz free energy. The interfacial distortions around ellipsoids and cylinders have quadrupolar geometry.[30, 21, 22] As a special case, of multipolar symmetry, cuboidal particles show that, in certain orientations, particles excite hexapolar, or octupolar modes, aside from quadrupoles in the interface.[31]

3 INTERPARTICLE INTERACTION AT THE INTERFACE

The conditions and limitations of assembly is governed by the interplay between the attractive and repulsive groups of forces, like the case of self-assembly in the bulk of the colloid. The common forces that exist in systems prone to self-assembly are attractive van der Waal forces, electrostatic double-layer repulsion, hydration repulsion, depletion forces, hydrophobicity, etc.[6] When the major opposing forces are comparable in magnitude and competitive with the variation of distance between the particles, such a system is said to be kinetically stable. Similarly, at interfaces, when energetics are favorable and particles get adsorbed to the interface, the interplay of the interparticle forces also becomes confined. The interaction among building units becomes more favorable along the direction of the interfaces, but less favorable through the direction of either phase.[32]. Self-assembly of colloidal particles at fluid interfaces is governed by both direct interactions, such as van der Waals and electrostatic interactions, and indirect interactions, such as forces due to overlap of interface distortions or capillary interactions.[23, 33]. The presence of a liquid bridge between two solid surfaces leads to an interaction through capillary force. The normal capillary-bridge forces can be attractive or repulsive depending on whether the capillary bridge is concave or convex, as a result of the shape of the liquid interface. When distortions from neighboring particles overlap, particles orient and migrate so that regions with like menisci charge overlap. In this way, the slope of the interface, and the area δA owing to the distortions, decreases. As particles approach, different parts of their distortion fields interact depending on their separation distance. These are called lateral capillary forces. The larger the interfacial deformation created by the particles, the stronger the capillary interaction between them. It is known that two similar particles floating on a liquid interface attract each other. [34] This attraction appears because the liquid meniscus deforms under the influence of gravity in such a way that the particles approach each other, especially for very small anisotropic particles as a result of electrostatic stresses, etc. Hence the origin of the flotation capillary force is the particle weight including the Archimedes force. In the case of nanometric non-isotropic particles, this flotation capillary force can be significant, due to the meniscus deformation by electrostatic stresses.[35] A force of capillary attraction appears also when the particles instead of being freely floating are partially immersed and confined into a liquid layer. [36, 37,38] The deformation of the liquid surface in this case is related to the wetting properties of the particle surface. This force is known as immersion capillary force. These two kinds of forces can be attractive or repulsive depending on the meniscus slope of the contact lines of the two particles. Capillary interaction energies between two particles can be calculated based on the difference between the changes of the fluid-fluid interface area for placing two particles at a given center-of-mass separation and for placing two isolated particles at a planar interface. The corresponding capillary interaction energy is [33],

$$\Delta E_{cap} = \gamma_{12}(\Delta A_{AB} - \Delta A_A - \Delta A_B) \quad (6)$$

where ΔA_{AB} is the change of the interface around the interacting particles, ΔA_A and ΔA_B are the changes of the interface areas around the single particles. Interface-mediated interactions follow power laws in the far-field and are thus long-ranged. In the near field, the interactions strongly depend on the particle shapes. To generalize further, in a system of N randomly oriented colloidal particles dispersed at a fluid-fluid interface, the (free) energy at the interface is given by [31, 39],

$$E_N(\Omega) = \gamma_{12}[S(\Omega) - A_{12} + A_{P1}(\Omega) \cos \theta_c] \quad (7)$$

where Ω represents the configuration of the particles. In general, any arbitrary anisotropic shape, the position and orientation are addressed by six parameters in 3D (cartesian positional and angular) so Ω is a function of 6N entries. When there are no particles

adsorbed at the interface $S(\Omega)$ is simply the total interfacial area A_{12} . However, when particles are trapped, the total fluid-fluid surface area alters (analogous to ΔA_{AB} for a two-particle system in Eq. 6). The total solid surface area of the particles wet by fluid 1 is $A_{P1}(\Omega)$ with a contact angle θ_c , E_N can be computed numerically for any configuration Ω in the near field, however analytical solutions for the interaction forces are available in the far field.[33, 39]

The strong deformation fields around anisotropic particles make them excellent vehicles for studying capillary interactions. The dynamics of microparticle assembly were first observed for ellipsoids at a water-oil interface a decade ago,[30] motivating interest in ellipsoidal particle assembly.[40, 41] The particles, with a major axis $10\mu m$ and minor axes $2\mu m$, interacted over distances as great as six particle lengths with weakly Brownian trajectories in the far-field, and well-determined paths in the near field. Particles approached in either tip-to-tip and side-to-side configurations. The former has a higher energy requirement than the latter. The tip-to-tip interactions follow the quadrupolar capillarity in the far field. For side-to-side arrangements, the simulation shows that contributions from higher-order modes are significant at longer separations.[41] Simulation of weakly nonspherical particles assuming pairwise additivity suggests that even nanometric deviation from sphericity can drive capillary assembly of ellipsoids into a variety of structures that include dendritic-trapped configurations, rafts, and hexagonal lattices.[42] Numerical calculations for two-particle, three-particle, and four-particle interactions predict a variety of stable and metastable configurations.[43]. Orthorhombic particles are a classic example where multiple stable orientations were found, depending on the particle aspect ratio and contact angles.[44] Anisotropic particles align as they migrate to preferred configurations. Interactions first occur because of their quadrupolar modes. Closer to contact, higher-order modes, near-field distortions, and the presence of corners and edges play roles in determining the strength of the interactions and the distance of the closest approach. Furthermore, rearrangement of wetting configurations and contributions from the associated solid-liquid wetting energies also play a role. Fig. 2 shows different types of assemblies formed from spherical and ellipsoidal particles of varying aspect ratios. He *et al.*[45] demonstrated that by controlling the interfacial energy between different liquids and suspended CdSe nanorods, the aspect ratio of the nanorods, and their concentration, the lateral packing of the nanorods can be varied. The proximity or packing of the particles is limited by particle roughness. Wavy contact lines pinned on the rough sites would create local disturbances near the particle, which is important only in the very near field.[46] When neighboring particles approach, these disturbances would interact. If they matched perfectly, with identical wavelengths, phases, and amplitudes, particles would attract. However, if they differed, as would be expected for random roughness, particles would be repelled. This concept was recently demonstrated using particles with wavy edges.[47] In the far field, these particles experience the usual capillary attraction. However, when distortions from the wavy contact lines overlap, particles with differing undulations are repelled. All of these have been discussed in prior literature.[48, 33, 39, 22, 40] As a bottom line, it can be said that depending on the particle orientation, position, and shape of the interface, subject to appropriate boundary conditions at the three-phase contact line, the fraction of the particles immersed in each phase can be established. These values have a significant effect on bulk fluidic properties such as viscous drag, radiation pressure force in optical trapping experiments, etc.[49]

4 EFFECT OF EXTERNAL FIELDS

The use of external fields to control particle suspensions has long been a powerful means for tailoring the mechanical, optical, and electronic properties of materials in various research[50] and applications.[51] They have also been used as efficient routes for self-assembly at interfaces.[52, 53, 54] The reason for this is that in a stable colloidal system, the particles are charged to hinder agglomeration, and the adsorption of particles at the interface is dynamic. This means that there is an inter-particle repulsion along with repulsion between the particle and fluid-fluid interface. When a charged particle approaches a fluid-fluid interface, it experiences repulsive image-charge forces, and the electrical double layers of the particles become strongly distorted by the proximity of the interface.[55] If such particles can be electrically or magnetically actuated, particle-interface contact becomes easier. More recently, external fields have emerged as key methods to direct the assembly of colloidal and nanoparticles. Electric or magnetic fields are obvious candidates for field-directed assembly. Colloidal and nanoparticle assembly in fields occurs due to induced interactions. Field-induced interactions in suspensions have been studied in detail for both magnetically and electrically polarizable colloids, due to their importance to magneto- and electrorheology. An article by Piao *et al.* explores the various stimuli-responsive polymer/inorganic hybrid materials fabricated by Pickering emulsion polymerization along with the rheological characteristics of smart fluids under electric (electrorheological) and magnetic (magnetorheological) fields.[56]

A field-responsive particle interacts with an external field due to its inherent permanent dipole, which is parallel to the major axis of the particle. When a field is applied normally to the interface, a resulting torque will tend to align the particle with the applied field, inducing a change in the orientation in case of a rod-like or ellipsoidal particle from parallel position to perpendicular. The external field adds a contribution to the free energy of the particle at the interface. Assuming that the external field has a generic form of $F_{ext} = -\vec{m} \cdot \vec{H}$ where \vec{m} and \vec{H} are the dipole moment and field strength respectively. If φ is the angle

between the field and dipole vectors, the free energy of the particle at the interface can be written as

$$\Delta E = (\gamma_{P1} - \gamma_{P2}) \cdot A_{P1} - \gamma_{12} \Delta A_{12} + \tau L - mH \cos \varphi \quad (8)$$

$\varphi = 0$ corresponds to the particle in the perpendicular (or vertical) orientation whereas $\varphi = \pi/2$ corresponds to the particle in the parallel (or horizontal) configuration. The line tension is expected to have a significant effect on the wetting properties of the nanoparticle only when the interfacial tension is very low, and when the three-phase line has a large curvature.[57]. The term pertaining to the displaced interfacial area (A_{12}) takes care of the eccentricity of the ellipsoids and hence the energy ultimately depends on the particle orientation. The less anisotropic the particle (lower aspect ratio) the larger the effect of the field. For particles with small anisotropy, the stable configuration is the perpendicular one, i.e., the particle aligns with the field. Obviously, in the limit of a spherical particle, the vertical orientation would be the preferred one, even for an external field of negligible strength. Thus, the presence of an external field imposes a preferred orientation on the particle, which tends to align with the field direction. For particles with intermediate anisotropy, the field will result in a configuration in which the particle is tilted at an angle θ to the interface. The change in the orientation of the particle, from the horizontal to the vertical orientation with field strength occurs in a discontinuous way. Hence, there is critical field strength at which the particle ‘jumps’ from a tilted configuration to a vertical one where the nanoparticle dipole points in the direction of the field. The critical field needed to induce the transition is strongly dependent on the nanoparticle size, aspect ratio, and interfacial tension.[28] Fig. 3 shows the relevant terms for spherical and cylindrical particles at fluid interfaces.

4.1 Magnetic field-induced assembly

Magnetic particles in an external field experience two types of forces; namely, the dipole-dipole interactions between particles and the dipole–field interaction. [58] The potential interaction between the magnetic moments \vec{m}_i and \vec{m}_j is given by,

$$U_{dd}(\vec{d}, \vec{m}_i, \vec{m}_j) = \frac{\vec{m}_i \cdot \vec{m}_j}{d^3} - 3 \frac{(\vec{d} \cdot \vec{m}_i)(\vec{d} \cdot \vec{m}_j)}{d^5} \quad (9)$$

where \vec{d} is the relative position of the dipoles. The strength of the dipole-dipole magnetic interaction between two identical particles can be characterized, as compared with thermal energy, by the magnetic coupling parameter Γ_m defined for two identical magnetic moments as

$$\Gamma_m = \frac{\mu_0 m^2}{16\pi r^3 k_B T}$$

where $\mu_0 = 4\pi \times 10^{-7} \text{NA}^{-2}$ is the free space permeability and $k_B T$ is the thermal energy, where k_B is Boltzmann’s constant and T is absolute temperature. For $\Gamma > 1$, the dipole-dipole interaction induces the formation of aggregates, due to precedence of magnetic coupling over thermal randomization. In case of spherical particles with remnant magnetization, the dipole-dipole potential induces the formation of linear, onion ring-like and cluster-like structures in the absence of an external magnetic field and at moderate temperatures.[59] In all these systems, the application of a uniaxial magnetic field induces a torque that tends to align and rearrange the self-assemblies along the imposed direction. Superparamagnetic particles only present magnetic dipole-dipole interactions under the influence of an external field. If the induced moments are coplanar with the relative position vector \vec{d} then

$$U_{dd}(\vec{d}) = \frac{\mu_0 m^2}{4\pi d^3} (1 - 3 \cos^2 \alpha)$$

where α is the angle between the dipole and the line connecting the dipoles which can range from $0 - 90^\circ$. The corresponding force is given by $F = \frac{3\mu_0 m^2 (1 - 3 \cos^2 \alpha)}{4\pi d^4}$. The dipole–dipole interaction is attractive when α is below 54.098° and repulsive when α varies from 54.098° to 90° . When two dipoles are aligned head-to-end, the dipole interaction is attractive, $F_{att} = -\frac{6m^2}{d^4}$. While they are aligned side by side, the net interaction is repulsive given by $F_{rep} = \frac{3m^2}{d^4}$. [60] Fig 4 shows the various forces between the magnetic particles.

At the critical angle of 54.098° the interaction approaches zero and Brownian motion tends to randomize the colloidal particles. However, when the dipole interaction energy is at least one order of magnitude greater than thermal energy the particles self-assemble into chain-like structures under the influence of external magnetic field. Along the magnetic field, the particles attract (F_{att}) each other and form chains due to head-to-end alignment of dipoles while the repulsive interaction (F_{rep}), results from

the side-by-side configuration of dipoles, keeping the chains apart. Thus tailoring of the spatial magnetic field allow control over both the global and local assembly behavior.[61] For in-plane rotating fields, the time-average of the dipolar interaction energy becomes attractive and holds when the applied field is rotating at high frequency, and the field periods are much shorter than the typical rotational and translational times of the adsorbed particles. If the field precesses at high frequency about the axis perpendicular to the interface, with a precession angle α_p , the dipole-dipole potential on the interface plane becomes,

$$\langle U_{dd} \rangle = - \frac{\mu_0 m^2 (1 - 3 \cos^2 \alpha_p)}{4\pi d^3}$$

4.1a Spherical particles

Magnetically responsive particles adsorbed at interfaces can be controlled by externally applied magnetic field when the magnetic energy is larger or comparable to the surface energy. However, the interfacial adsorption does not have any significant effect on the long-range magnetic interaction between particles, since it not screened or altered by changes in the distribution of magnetic particles. The external magnetic field generates a magnetic torque $\bar{\tau}_m = \bar{m} \times \bar{H}$ that is counterbalanced by the viscous torque which is the torque generated by the contact line friction, and interfacial torque is given by $\tau_{int} \propto \gamma_{12} r^2 \alpha_t$ where α_t is the torsion angle. [62] The adsorbed particle rotates about an axis parallel to the fluid interface when magnetic energy overcomes the surface energy which occurs when the fluid-fluid interfacial tension is low, the strength of the magnetic field is large and/or the particles are small but intensely responds to the applied field. The interfacial torque depends on the size squared; hence one would expect that small nanoparticles can be more easily reoriented when adsorbed at a fluid interface. However, small particles often have smaller permanent moments and display a weaker response to the applied fields. By subjecting to strong magnetic fields, this limitation can be overcome.[63] For ferro/ferrimagnetic particles adsorbed at a fluid interface, the interfacial torques are usually larger than the magnetic torques. Constraining the system by perpendicular orientation of the magnetic field prevents out-of-plane rotation of the trapped particles. [48]

An oscillating out-of-plane field (having frequency ω), $H e^{i\omega t}$ causes the particles to execute a rotational motion and the magnetic torque $\tau_0 e^{i\omega t}$ and deforms the fluid interface displacing the three-phase contact line due to the oscillatory rotation given by $\varphi_0 e^{i(\omega t + \delta\omega)}$. As a result, the adsorbed particles synchronously rotate with the applied field.[63]. A novel method of trapping magnetic particles by magnetic tweezers to probe the wetting at the interface as a result of the torques generated was proposed by Cappelli *et al.*[63] The angular orientation of the particles was studied as a function of time when the particles are subjected to varying torques. At lower torques, the particle deforms the interface up to the point where it overcomes the contact line pinning. Such kind of wetting phenomena is known as dynamic wetting, as opposed to static wetting for the trivial case. This limiting configuration depends on the particle surface properties and interfacial tension. At higher torques, the contact line displaces at different rotational speeds. Cappelli[64] demonstrated an interfacial rheometry technique based on periodic attraction and repulsion between pairs of micrometer-sized magnetic particles regulated by controlling the dipole forces by Intra-Pair Magnetophoresis (IPM) (Fig. 5(a)).[65] The interfacial drag coefficient, ζ_r was obtained from the particle displacements (which is in μm), forces (pN) and velocities ($\mu m/s$) using the methodology mentioned in van Reenen *et al.*[65] When the magnetic field is applied normally to the interface, the force between particles at close proximity is repulsive. At low Reynolds number regime ($Re \ll 1$), the dipole-dipole interaction is limited by the hydrodynamic drag. In the limiting case, the magnetic torque is balanced by the hydrodynamic torque i.e. $mH \sin \varphi = \zeta_r \varphi$. The solution to this equation gives the time dependence of the angle between the field and the magnetic moment. When the field is changed to in-plane configuration (parallel to the interface) then dipole-dipole interaction becomes attractive. The application of stronger magnetic fields or higher magnetic susceptibility of the particles revealed non-linear responses of the interface. Using the competitive balance of the magnetic and interfacial forces on the trapped spherical paramagnetic colloid, Tsai *et al.* reported a microfluidic interfacial tensiometry technique to measure ultralow interfacial tensions up to $10^{-5} - 10^{-6} Nm^{-1}$.[66] The assembly at the interface in such a case is reversible, as reported by Martinez *et al.* for linear aggregates of micrometer-sized magnetic particles. Disassembly of the particles occurs when the applied field is abruptly tilted out of the confining surface (out-of-plane motion). The chains of laterally aggregated particles "unzips" causing partial fragmentation of the chains and gradual separation of the monomers and the abrupt colloidal explosion.(Fig 5(b)) Chains and bundles disintegrate due to thermal fluctuations as soon as the applied field is switched off.[54] 2D ordering of supermagnetic colloidal particles at the interface shows two-fold melting transitions were observed from solid to liquid phase with an intermediate hexatic phase as described by Zahn *et al.*(Fig. 5(c))[53]. Similarly, Wen *et al.*[67] reported 2D colloidal crystal ordering by applying perpendicular fields. The balance between the repulsive magnetic interaction and the attractive interaction due to the weight of the particles projected along the surface tangent, yielded triangular, oblique, rectangular and square lattice structures. By using two

different-sized magnetic particles, local formations five-fold symmetrical structures were also achieved. These lattice structures were tunable by adjusting the polar and azimuthal angles of the magnetic field relative to the surface normal. Grosjean et al. [68] investigated similar triangular latticing for millimetric particles on a fluid interface when capillary attraction on a curved interface is balanced by the dipolar repulsion. Depending on the number of particles in the assembly and the amplitude and orientation of the imposed magnetic fields, including oscillatory fields, a variety of structures can be observed. [68] Similar results were reported by Froltsov et al.[52] using gradually tilting fields on crystal lattices of 2D superparamagnetic particles, confined to a planar liquid-gas interface using a lattice sum minimization model. When the field is directed perpendicular to the liquid-gas interface, a repulsive interaction acts between the particles leading to stable triangular crystals. By tilting the external field, the interaction becomes anisotropic, and a mutual attraction appears upon a threshold tilt angle. Various stable crystal lattices including rectangular, oblique, chain-like oblique, and rhombic structures were obtained by varying the tilt angle, the colloidal density, and the strength of the magnetic field. Lefebvre reported the formation of chains and compact circular aggregates of magnetic nanoparticles under perpendicularly applied magnetic fields larger than 60 mT at air–water interface as a result of a balance between van der Waals and magnetic dipole–dipole interactions.[69] Maintaining a magnetic field gradient at liquid-air interface yields tunable hexagonally ordered clusters of macroscopic ferromagnetic particles as reported by Golosovsky et al.[70] The particles assemble into hexagonally ordered clusters with magnetically tuned lattice constants. Han *et al.*[71] reported self-assembly of synchronized ferromagnetic spinners at air-water interface under rotating magnetic field applied in-plane of the interface. A low-frequency alternating field applied parallel to the fluid interface, induces the formation of pearl-like-chains that aggregate and fragment depending on the dimensionless Mason number given by,

$$Mn = \frac{\eta\dot{\gamma}}{\mu_0 m^2}$$

which is the ratio of the viscous force and dipolar attraction and $\dot{\gamma}$ is the shear rate. [71] The interaction between the spinners yields dynamic phases and lattices which exhibit self-healing behaviour. The ordering and dynamics of the spinner lattice are tunable by varying the field characteristics. At high field frequency, particles self-assemble in dynamic planar structures due to isotropic potential as in Eq. 9. At different amplitudes and frequencies of the field, different types of aggregates are formed such as pulsating clusters, linear aggregates and spinners. These spinners self-assemble and synchronously rotate by the in-plane rotating field and the flow generated induces the development of dynamic crystalline lattices that show self-healing behavior (Fig 5(d)).[71, 72] Notable work by Snezhko et al. demonstrated dynamic snake-like self-assemblies of ferromagnetic particles by application oscillating field normal to the air-water interface. The segments of the snake exhibit long-range antiferromagnetic ordering, whereas each of these segments is again ferromagnetically aligned. They report an effective exchange interaction to explain this observation. [73].

4.1b Non-spherical particles

Bresme and Newton et al. studied the influence of magnetic fields on cylindrical[74] and ellipsoidal magnetic particles[75, 62] at liquid interfaces. Bresme et al.[75] demonstrated a thermo-dynamical model which determines the orientation and free energy of ellipsoidal magnetic particles under magnetic field directed perpendicular to the interface. Aspect ratio, particle size and external field strength play crucial roles in this regard. There exists a critical field strength for which the particle undergoes discontinuous transition from a configuration where the major axis (dipole moment) is tilted with respect to the interface, to a configuration where the axis is aligned with the external field (Fig 6(a)). Calculations showed that the critical field needed to induce the transition is strongly dependent on the nanoparticle size, aspect ratio and interfacial tension. Monte Carlo simulations set up using orientation-dependent interaction between the nanoparticles and the liquid for varying magnetic fields, corroborated with the observation of discontinuous transition. Further improvements by considering the interface deformation as well was given by Newton et al.[62] and Davies[76, 77] using lattice Boltzmann method. Davies *et al.*[77] showed that application of a strong magnetic field perpendicular to the fluid interface can be used to control the capillary assembly process of micro ellipsoids. Simulations showed that the ellipsoidal orientation is determined by the surface tension of the interface, strength of the field and the magnetic moment of the particle. The dipole-dipole interactions can be neglected compared to the capillary interactions owing to the weak magnetization of the ellipsoids. Anisotropic structures termed as "capillary caterpillars" were observed as a result of side-by-side packing of the particles due to the dynamically changing capillary strength by the external field.(Fig. 6(b))The discontinuous switching behaviour of the particles is useful in applications of photonic systems that require dynamic control of optical properties such as in electronic readers[78] For cylindrical particles, Newton[74] demonstrated a similar transition. However, in this case by tuning both the aspect ratio and contact angle of the cylinder, subjected to external magnetic field, multiple locally stable orientations were obtained through non-volatile transitions.(Fig 6(c)) The rotational motion of ferromagnetic nickel nanowires at the interface under magnetic field were used to probe the nonlinear micro-rheology of layers of protein lysozyme adsorbing at air-water interface.[79] In that case, deviations from Eq. 9 will occur due to non-linear responses.[80] Unconventional

shaped micro-rafts (50 μ m radius) with sinusoidal edge-height profiles under rotating magnetic field applied parallel to the interface, generate interesting assembly configurations owing to the near-field repulsive and attractive capillary interactions competing with torque generated via the rotating field. This induces a programmable self-assembly depending on the rotational velocity and the peripheral profile of the magnetic rafts(Fig 6(d)).[81]

4.2 Electric field induced assembly

Particles are polarized under an electric field, and the dipole-dipole interaction between them causes assembly, similar to the previous case of magnetic field. For a pair of identical spherical particles, the dipole-dipole interaction energy is

$$U_{dd}(\bar{d}, \alpha) = m\beta E \left[\frac{3 \cos^2 \alpha - 1}{(d/2r)^3} \right] = m\beta E (2r/d)^3 P_2(\cos \alpha) \quad (10)$$

If α is the angle as defined earlier, $\beta = \frac{\epsilon_p - \epsilon_s}{\epsilon_p + 2\epsilon_s}$ where ϵ_p and ϵ_s are the dielectric constant of the particle and solvent respectively, m is the electric dipole moment of the particle in response to the electric field E . P_2 is the second Legendre polynomial. Electric coupling parameter Γ_e can be defined as $\Gamma_e = \frac{\pi \epsilon_0 \epsilon_s (\beta E)^2 r^3}{k_B T}$ where ϵ_0 is the free space permittivity. U_{dd} is attractive if the line joining the two dipoles is parallel to the electric field whereas it is repulsive for perpendicular alignments. Solving the Laplace equation $\nabla^2 U_{dd} = 0$ the force is calculated to be $\frac{rF}{k_B T} = \frac{3}{4} \Gamma_e \bar{f}$ where $\bar{f} = \left(\frac{2r}{d}\right)^4 [\widehat{e}_d (2f_{\parallel} \cos^2 \alpha - 2f_{\perp} \sin^2 \alpha) + \widehat{e}_{\alpha} (2f_{tor} \sin 2\alpha)]$ where f_{\parallel} , f_{\perp} and f_{tor} are the parallel, perpendicular and torsional force components respectively, which are function of dielectric constants, particle size and radial distance. \widehat{e}_d and \widehat{e}_{α} are the unit vectors for the radial and angular components. The interaction is attractive, $F_{att} = -\frac{3}{2} \Gamma_e \left(2r/d\right)^4$ if the line joining the dipoles is parallel to the electric field whereas it is repulsive, $F_{rep} = -\frac{3}{4} \Gamma_e \left(2r/d\right)^4$ for perpendicular alignments.[82] These terms are calculated considering point dipole limitation where the force components are unity.[83] If the particle and the solvent both polarize under electric field to the same extent (i.e. $\epsilon_p = \epsilon_s$) then $\beta = 0$ and consequently the interaction force goes to zero. when $\epsilon_p \neq \epsilon_s$, excess bound charge appears on the particle surfaces under the electric field, such that far from the particle it appears as a point dipole with dipole moment $m = 4\pi \epsilon_0 \epsilon_s \beta E r^3$. [58] Other than that, mobile charges, such as those in an electrostatic double layer also respond to applied fields and can contribute to the polarization.[84] However in the far-field, the induced field surrounding a polarized particle takes the form of a dipole and leads to a strong dipole-dipole interaction between particles. When the interaction is sufficiently strong to overcome Brownian motion (the relative strength characterized by Γ_e), particles will initially start to assemble and consequently form large clusters with distinct ordered structuring. Ideally, the coarsening proceeds to form the lowest energy structure, a body-centered tetragonal (bct), hexagonally close-packed (hcp), or face centered cubic (fcc) lattice, depending on the particle concentration and field. [85]

Particles trapped at interfaces, when acted upon by an external electric field experience an electrostatic force normal to the interface and since the particles become polarized, they also repel each other due to the dipole–dipole interactions. For a trapped particle at interface, there is a mismatch of dielectric constants on the top and bottom halves, depending on the nature of two fluids involved. If the interface does not contain any particles, the electric field is normal to the interface and its intensity in the lower and upper fluids is constant, while changing discontinuously at the interface. When there are other particles present at the interface they interact with each other via dipole-dipole interactions. The magnitude and dominance of electrostatic interaction along with capillary forces governs the assembly at interfaces. For a charged particle, the Coulombic force is also important. Charged particles are efficiently mobilized by external electric fields, which is characterized by the electrophoretic mobility of the particles. In case of particles in bulk, the electrostatic interaction among polarized particles causes the particles to cluster in the direction of the electric field. However, at the interface this interaction is repulsive. Electric fields affect a collection of dispersed particles according to the properties of both the particles and the medium. Electric field also plays an important role in governing the contact angle via the voltage variation or electrowetting.[86] The change in the contact angle cause the particle to move normal to the interface to satisfy the new contact angle requirement. The electric field strength, particle geometry (isotropic/anisotropic), and field frequency are all controllable parameters important for the interfacial self-assembly. The mechanisms that can polarize the particles vary for the different media and for direct and oscillating fields. The relative polarizability of particles and the solvent, distribution of mobile (e.g. dispersed ions in case of additive electrolytes) and immobile charges (e.g. covalently bound surface charges), all play important roles in the particles' response to electric fields.

4.2a Spherical particles

Aubry et al. demonstrated electrically controlled monolayer packing of spheres at interfaces when a DC electric field is applied perpendicular to the interface.[87] For an isolated particle at interface acted upon by an electric field, the force acting normal to the interface has been numerically computed to be

$$F_{ev} = r^2 \epsilon_0 \epsilon_U \left(\frac{\epsilon_L}{\epsilon_U} - 1 \right) E^2 f_v \quad (11)$$

Where f_v is a dimensionless vertical force coefficient, ϵ_U and ϵ_L are the dielectric constants of the upper and lower fluid in contact. The factor in the bracket of Eq. (11) disappears in the case of an isolated particle submerged in a single fluid. Hence it does not experience a force field under bulk condition. F_{ev} is also dependent on the particle radius and the dielectric constants of the fluids in contact. It may be directed along or opposite to the buoyant weight of the particles depending on these parameters. The lateral electric force acting on the particle due to its neighboring particle-particle interactions is

$$F_{el} = \epsilon_0 \epsilon_U \left(\frac{\epsilon_L}{\epsilon_U} + 1 \right) r^2 E^2 \left(\frac{r}{d} \right)^4 f_l \quad (12)$$

where f_l is the dimensionless lateral force coefficient. As mentioned earlier, F_{el} is repulsive and causes particles to move away from each other. The repulsive force thus depends on the sixth power of particle radius r and on the fourth power of the inverse of the distance d between the particles. This force was shown to be stronger than the random Brownian force, indicating that an electric field can indeed be used to manipulate small particles within a two-fluid interface. The normal electric force alters the particles' position at the interface, deforming the interface further causing eventual attractive lateral capillary force which is given by,[32, 24, 52, 40,88]

$$F_{lc} = - \left(-\epsilon_0 \epsilon_U \left(\frac{\epsilon_L}{\epsilon_U} - 1 \right) r^2 E^2 f_v + \frac{4}{3} \pi r^3 \rho_p g f_b \right)^2 \frac{1}{2\pi\gamma d} \quad (13)$$

where ρ_p is the particle density and f_b represent the buoyancy force coefficient. The first part of the above expression is the vertical force F_{ev} mentioned earlier.

Fig 7. depicts the above-mentioned forces for a pair of spherical particles. The first term varies as the fourth power of the particle radius and the second term as its sixth power, making the contribution of the particle's buoyant weight for micron and nanometric particles negligible. Thus, it is unlikely for uncharged particles to self- assemble under mere capillarity. However, charged particles[89] or occurrence of irregular contact lines cause self-assembly at this dimension.[38] This restriction is overcome by an electric field of $O(10^6)$ V/m when the particles experience electric force normal to the interface of at least an order of magnitude higher than the random Brownian force, which is the order at which capillary forces become significant.[90] The repulsive F_{el} is short-ranged (varying as d^{-4}) whereas attractive F_{lc} is long-ranged(varying as d^{-1}). Therefore, at the equilibrium distance for a fixed field strength, the net force acting on the particle is zero. The force balance leads to the following dimensionless equilibrium separation $d_{eq}/2r$ between two isolated particles given by,

$$\frac{d_{eq}}{2r} = \frac{1}{2} \left(\frac{2\pi\epsilon_0\epsilon_U\left(\frac{\epsilon_L}{\epsilon_U}+1\right)\gamma E^2 f_l}{r\left(-\epsilon_0\epsilon_U\left(\frac{\epsilon_L}{\epsilon_U}-1\right)E^2 f_v + \frac{4}{3}\pi r^3 \rho_p g f_b\right)^2} \right)^{1/3} \quad (14)$$

Thus varying the electric field intensity, the equilibrium distances between particles vis-a-vis the assembly and monolayer packing at interface can be controlled. Aubry [87] reported an excellent correlation of the equilibrium distances between the experimental results of particles at oil-water interface along with theoretical calculations where the force coefficients are obtained numerically (Fig 8(a)).[91] Two quantities, namely Bond and Weber numbers are used to define the force balance of the sphere at the interface given by $BO = \frac{gr^2\rho_L}{\gamma}$ and $WE = \epsilon_0\epsilon_U\left(\frac{rE^2}{\gamma}\right)$ respectively. When BO approaches zero, i.e. for small (nanometric) particle sizes, the interfacial deformation due to the particle weight is minimal. As radii approach $10\mu m$ the deformation become significant.[92] As mentioned earlier, in presence of a high enough electric field, F_{lc} for nanometric particles becomes significant even when the BO approaches zero. [90, 24].

Liu *et al.* demonstrated the coalescence of liquid water marbles driven by a high DC electric field assisted by stabilizing silica particles. The threshold voltage for coalescence was shown to depend on the stabilizing particles as well as on the surface tension of the aqueous phase. The increase in voltage is directly proportional to the number of marbles coalescing.[93] It has been reported that DC electric fields can induce strong currents in the electrolyte, which may degrade the material and interfere with the distribution of free charge carriers. Therefore, most experiments employing DC fields focus on poorly conducting liquids or low electric fields. To avoid such restrictions, high-frequency AC electric field are often used to polarize only the solid dielectric particles, leaving the ionic double layer or capacitive charges unaffected, as redistribution of charges require a finite response

time[94]. Force experienced by a particle at an interface subjected to AC fields is similar to that of DC. Eq. 11 then represents the time-averaged force in an AC field with E as the RMS value for an AC electric field. When a spherical particle is subjected to a non-uniform electric field, and its dielectric constant is different from that of the fluid, the electric stress acting on its surface results in a net force, referred to as the Dielectrophoretic or DEP force which causes the particle to translate. If a particle is sufficiently small compared to the length scale over which the non-uniform electric field varies, the field gradient is considered to be constant, the time averaged DEP force acting on a spherical particle in an AC electric field is given by [95]

$$F_{DEP} = 2\pi r^3 \epsilon_0 \epsilon_s \beta(\omega) E_{RMS} \nabla E_{RMS} \quad (15)$$

where E_{RMS} is the RMS value of the field, $\beta(\omega)$ is the real part of the frequency dependent Clausius-Mossotti factor (similar to the β defined earlier) given by $\beta(\omega) = Re \left(\frac{\epsilon_p^* - \epsilon_s^*}{\epsilon_p^* + 2\epsilon_s^*} \right)$ where ϵ_p^* and ϵ_s^* are the frequency-dependent complex permittivities of the particle and the solvent, respectively. The Weber number in this case becomes $WE = \epsilon_0 \epsilon_U \beta(\omega) \left(\frac{rE^2}{\gamma} \right)$. For a particle at a two-fluid interface, the DEP force differs from the expression on Eq. 15. The Clausius-Mossotti factor $\beta(\omega)$ depends on the dielectric constants of the particle and the two fluids involved, and on the orientation of the particle within the interface as well. The third factor again depends on the wettability and the buoyant weight of the particle. There are quite a few examples of the use of electric fields to manipulate assembly of particles at interfaces of Pickering droplets by the dielectrophoresis (DEP) effect. Nudurupati *et al.* [96] demonstrated the influence of an externally applied uniform AC electric field on the distribution of particles on the surface of a drop immersed in another immiscible liquid with a finite dielectric constant difference. When a drop of liquid is placed in a liquid with a smaller dielectric constant value, particles distributed on the surface of the drop get collected at the poles of the elongated drop. On the other hand, when the dielectric constant of the suspended drop is smaller, particles collect in a ring-shaped region near the equator. It is shown that the motion of particles is due to the DEP force that acts because the electric field on the surface of the drop is nonuniform, even when the drop is subjected to a uniform electric field. They also corroborate the findings with simulations results that show that the electric field strength is maximal at the equator when the dielectric constant of the drop is smaller than that of the ambient liquid and therefore the particles for which the Clausius-Mossotti factor is positive should, in a first-order approximation, collect in a ring-shaped region near the equator. On the other hand, when the dielectric constant of the suspended drop is greater, the electric field strength is maximal at the poles, and thus particles for which the Clausius-Mossotti factor is positive collect at the poles. Moreover, when particles get collected at the poles of a drop, the electric field strength required to break the interface stability is smaller than the case without particles. This is due to the reduction of interfacial tension at poles due to the trapping of the particles (Fig 8(b)). Hwang *et al* demonstrated that along with manipulating the particle distribution on drop surfaces, the Pickering emulsions could be destabilized. It was shown that proximal droplets could merge from the spaces on the drop surface that was left uncovered by the particles.[97]. In a later work, Nudurupati[98] *et al.* investigated the dependence of F_{DEP} on the particles' and drop's radii and the dielectric properties of the fluids and particles. When the drop radius is larger than a critical value it is not possible to concentrate particles on the interface as the drop breaks at an electric field intensity smaller than that needed for concentrating particles. F_{DEP} varies inversely with the drop radius hence, the spatial concentration manipulation is effective with a decreasing drop size. Particles experiencing positive dielectrophoresis can be segregated from those experiencing negative dielectrophoresis on the surface of a drop, forming a localization of one kind at the poles and the other at the equator. Further, one type of particles can be eliminated from the drop surface by tuning the field intensity(Fig 8(c)). Dommersnes *et al.* [99] have shown that electric fields induce structural assembly of colloidal armour on oil drops in the form of 'equatorial' ribbons and 'longitudinal' dipolar chains. Electrohydrodynamic circulation flows inside the drop and dipole interaction between particles account for the observations.[100] The armour width can be actively controlled by the strength of the electric field and this effect is intimately linked to the magnitude of polarizability contrast between particles and the drop oil and colloidal particle conductivity.

4.2b Non-spherical particles

Crassous *et al.*[94] combined experimental and computational studies to demonstrated that ellipsoidal particles can reversibly self-assemble into regular tubular structures when subjected to an AC electric field. The effect of aspect-ratio or the particle shape, and the field-induced dipolar interactions have been demonstrated with the help of model calculations. The ellipsoids can be reversibly assembled into well-defined microtubular structures. In the presence of a sufficiently strong electric field, experiments show that certain alignments of anisotropic colloids that are stable without electric field become unstable under an electric field. For example, two rods align with their ends touching and the stable alignment in which their long sides face each other is no longer stable. This is due to an electrostatic torque $\vec{\tau}_e = \vec{m} \times \vec{E}$ normal to the interface that acts on the rods. Experimental evidence by Janjua *et al* [101] reveal that an external electric field normal to a fluid-fluid interface is effective in aligning rods floating on

the interface and vis-a-vis the lattice spacing of the formed monolayer. In presence of an electric field, a rod floating on the fluid interface experiences similar electric force and torque as in case for spherical particles. The electric force affects the approach velocity of the rods, and the torque aligns the rods parallel to each other. In presence of electric field of sufficient strength (5000 V), rods of the monolayer align end-to-end and the lattice spacing of a self-assembled monolayer of rods increases (Fig. 8(d)). This equilibrium arrangement is independent of their initial orientation. Similar to the previous case of spheres, the electric field causes a rod on the interface to experience an electrostatic force normal to the interface. In addition, in an electric field the rods become polarized and interact with each other via dipole–dipole interactions. This results in repulsive force and torque. The equilibrium distance between the rods is determined by the balance of the attractive capillary forces and the repulsive dipole–dipole forces.

5 Conclusions and Outlook

This article provides an outline of research for field-assisted assembly of particles at fluid–fluid interfaces. Interest in interface-assisted assembly has grown manifold over the years. With the advancements in synthesis techniques for nanoparticles, investigations have been carried out for various shapes, sizes and surface functionalities. Particle shape plays a significant role in deciding the energy landscape at the interface. We first discussed the case of isolated particles at interface. Deviation from sphericity induces various stable and metastable states of the particles at interface. The most reported systems are those of rod-like or ellipsoidal particles. Interparticle interaction between the particles is again shape dependent. Interfacial deformation caused by anisotropic particles are multipolar in nature owing to the orientation and position of the particles. The overlap of the deformations of the interface in the near field cause the modification of the three-phase contact line, resulting in capillary interactions. For shape anisotropic particles, higher order deformations such as hexapolar or octupolar are obtained for certain particle orientations. The important physical aspects of the above-mentioned categories have been highlighted along with reports and results from the relevant case studies. The presence of field acts as an additional tool for tuning the assembly at interface. In this regard, the two important external influences of electric and magnetic field have been discussed. First a general formalism of the effect of an external field is provided where the particle’s inherent dipole moment interacts with the spherical and cylindrical particles. Then, the interaction of the particle with the external field has been demonstrated. The two cases of spherical and non-spherical particles are discussed along with relevant examples from literature. The use of external fields to assist assembly at fluid–fluid interfaces holds immense potential in terms of designing assembly at interfaces. Contrary to the traditional use of micrometric sized particles, nanoparticles have gained importance over the years for their ease of synthesis and functionalization. Novel synthesis methods allow physical properties such as microwave or optically responsivity to be incorporated into the nanoparticles. These particles then become markers with potential in investigation of collective behaviour at interfaces under various physico-chemical conditions. Moreover, biocompatible nanoparticles serve as biomarkers allow monitoring of drug assimilation at bio-interfaces or membranes. Magnetic nanoparticles have also shown to hold advantage for targeted drug delivery in a cargo pick-up-drop fashion [102] Nanoparticle shape is another interesting aspect that provide ample opportunities for further work. The short-range interactions could be modified by use of further anisotropic colloids and other hybrid constructs. Long-range electric and magnetic interactions can again be coupled in various degrees to further increase the complexity of the dynamical structures at the interface.

REFERENCES

- [1] George M. Whitesides and Mila Boncheva. 2002 *Proceedings of the National Academy of Sciences* **99** 8.
- [2] John A. Rogers et al. 2001 *Proceedings of the National Academy of Sciences* **98** 9.
- [3] Chantal Paquet and Eugenia Kumacheva 2008 *Materials Today* **11** 4.
- [4] W.A. Gifford and L.E. Scriven 1971 *Chemical Engineering Science* **26** 3.
- [5] R H Ottewill et al 1997 *Colloid and polymer science* **275** 3.
- [6] Jacob N. Israelachvili. 1991 *Intermolecular and surface forces* (Academic Press London)
- [7] Ramsden W. 1904 *Proceedings of the Royal Society of London* **72**.
- [8] Spencer Umfreville Pickering 1907 *J. Chem. Soc. Trans.* **91** 0.

- [9] Pawel Pieranski 1980 *Phys. Rev. Lett.* **45** 7
- [10] G. Sreenivasulu et al 2014 *Applied Physics Letters* **104** 5.
- [11] Guido Avvisati, Teun Vissers, and Marjolein Dijkstra. 2014 *The Journal of chemical physics* **142** 8.
- [12] Junaid Qazi, Göran Karlsson, and Adrian Rennie. 2011 *Progress in Colloid and Polymer Science*, **13** 8.
- [13] Margaret Rosenberg et al. 2020 *Soft Matter* **16** 18.
- [14] Shan Jiang et al. 2010 *Advanced materials* **22** 10.
- [15] Anna Wang et al. 2016 *Soft Matter* **12** 43.
- [16] Peter A. Kralchevsky and Kuniaki Nagayama. 2000 *Advances in Colloid and Interface Science* **85** 2.
- [17] Krassimir Velikov et al. 2002 *Applied Physics Letters* **80** 1.
- [18] Zhen Wang et al. 2018 *Expert Opinion on Drug Delivery* **15** 4.
- [19] Maxim V. Gorkunov and Mikhail A. Osipov. 2011 *Soft Matter* **7** 9.
- [20] Takehiro Yamamoto, Takanori Suga, and Noriyasu Mori. 2005 *Phys. Rev. E* **72** 2.
- [21] Eric P. Lewandowski et al. 2010 *Langmuir* **26** 19.
- [22] Lorenzo Botto et al. 2012 *Soft Matter* **8** 39.
- [23] F Bresme and M Oettel. 2007 *Journal of Physics: Condensed Matter* **19** 41.
- [24] Anna Wang, W. Benjamin Rogers, and Vinothan N. Manoharan. 2017 *Phys. Rev. Lett.* **119** 10.
- [25] Eric P. Lewandowski et al. 2009 *Soft Matter* **5** 4.
- [26] Lu Yao et al. 2015 *Journal of Colloid and Interface Science* **449**
- [27] Michael J. Solomon and Patrick T. Spicer. 2010 *Soft Matter* **6** 7.
- [28] Jorge L. C. Domingos, François M. Peeters, and W. P. Ferreira. 2018 *PLOS ONE* **13** 4.
- [29] Jordi Faraudo and Fernando Bresme. 2003 *The Journal of Chemical Physics* **118** 14.
- [30] J. C. Loudet et al. 2005 *Phys. Rev. Lett.* **94** 1.
- [31] Giuseppe Soligno, Marjolein Dijkstra, and Rene van Roij. 2016 *Phys. Rev. Lett.* **116** 25.
- [32] Yoon Lee. 2007 *Self-Assembly and Nanotechnology: A Force Balance Approach* (Wiley)
- [33] Dimitris Stamou, Claus Duschl, and Diethelm Johannsmann. 2000 *Phys. Rev. E* **62** 4.
- [34] W.A. Gifford and L.E. Scriven. 1971 *Chemical Engineering Science* **26** 3.
- [35] Shemaiah M. Weekes et al. 2007 *Langmuir* **23** 3
- [36] P.A Kralchevsky et al. 1992 *Journal of Colloid and Interface Science* **151** 1
- [37] V.N. Paunov et al. 1992 *Colloids and Surfaces* **67**.
- [38] P. A. Kralchevsky, V. N. Paunov, and Kuniaki Nagayama. 1995 *Journal of Fluid Mechanics* **299**
- [39] Krassimir D. Danov et al. 2005 *Journal of Colloid and Interface Science* **287** 1
- [40] L. Botto et al. 2012 *Soft Matter* **8** 18.
- [41] Jean-Christophe Loudet and Bernard Pouligny. 2011 *The European physical journal. E, Soft matter* **34** 76.
- [42] F Bresme and M Oettel. 2007 *Journal of Physics: Condensed Matter* 19.41
- [43] J.B. Fournier and P. Galatola. 2002 *Phys. Rev. E* 65 3
- [44] G. Morris, S.J. Neethling, and J.J. Cilliers. 2011 *Journal of Colloid and Interface Science* **361** 1.
- [45] Jinbo He et al. 2007 *Small* **3** 7.

- [46] Jacob Lucassen. 1992 *Colloids and Surfaces* **65** 2.
- [47] Lu Yao et al. 2013 *Soft Matter* **9** 3.
- [48] Ping Liu et al. 2015 *Soft Matter* **11** 31.
- [49] David G Grier. 1997 *Current Opinion in Colloid and Interface Science* **2** 3.
- [50] Bartosz A. Grzybowski et al. 2017 *Chem. Soc. Rev.* **46** 18.
- [51] Markus Niederberger. 2017 *Advanced Functional Materials* **27** 47.
- [52] Eric P. Lewandowski et al. 2009 *Soft Matter* **5** 4.
- [53] K. Zahn, R. Lenke, and G. Maret. 1999 *Phys. Rev. Lett.* **82** 13.
- [54] Fernando Mart´inez-Pedrero et al. 2020 *Journal of Colloid and Interface Science* **560**
- [55] E C Mbamala and H H von Grnberg. 2002 *Journal of Physics: Condensed Matter* **14** 19
- [56] Shang Hao Piao et al. 2015 *Soft Matter* **11** 4
- [57] Fernando Bresme and Nicholas Quirke. 1999 *The Journal of Chemical Physics* **110** 7
- [58] John David Jackson 1999 (3rd edition) *Classical Electrodynamics* Wiley.
- [59] Fernando Martinez-Pedrero, Andrejs Cebers, and Pietro Tierno. 2016 *Phys. Rev. Applied* **6** 3.
- [60] Jianping Ge et al. 2011 *Nanoscale* **3** 1
- [61] S. Sacanna and A. P. Philipse. 2006 *Langmuir* **22** 24.
- [62] Bethany J. Newton, Kenneth A. Brakke, and D. Martin A. Buzza. 2014 *Phys. Chem. Chem. Phys.* **16** 47.
- [63] S. Cappelli 2016 PhD thesis (Eindhoven University, Department of Biomedical Engineering).
- [64] Stefano Cappelli et al. 2016 *Soft Matter* **12** 25.
- [65] Alexander van Reenen et al. 2013 *Applied Physics Letters* **103** 4.
- [66] Scott S. H. Tsai et al. 2013 *Lab on a Chip* **13** 1.
- [67] Weijia Wen, Lingyun Zhang, and Ping Sheng. 2000 *Phys. Rev. Lett.* **85** 25.
- [68] G. Grosjean, M. Hubert, and N. Vandewalle. 2018 *Advances in Colloid and Interface Science* **255** 84.
- [69] S. Lefebure et al. 1998 *The Journal of Physical Chemistry B* **102** 15.
- [70] M. Golosovsky, Y. Saado, and D. Davidov. 2002 *Phys. Rev. E* **65** 6.
- [71] Koohee Han et al. 2020 *Science Advances* **6** 12.
- [72] Guido Avvisati, Teun Vissers, and Marjolein Dijkstra. 2014 *The Journal of chemical physics* **142** 8.
- [73] A. Snezhko, I. S. Aranson, and W.-K. Kwok. 2006 *Phys. Rev. E* **73** 4.
- [74] Bethany J. Newton and D. Martin A. Buzza. 2016 *Soft Matter* **12** 24.
- [75] Fernando Bresme and Jordi Faraudo. 2007 *Journal of Physics: Condensed Matter* **19** 37.
- [76] Gary B Davies et al. 2014 *Soft Matter* **10** 35.
- [77] Gary B. Davies et al. 2014 *Advanced Materials* **26** 39.
- [78] Shin-Hyun Kim et al. 2011 *NPG Asia Materials* **3** 1.
- [79] Daniel B. Allan et al. 2014 *Soft Matter* **10** 36.
- [80] Prajnaparamita Dhar et al. 2010 *Phys. Rev. Lett.* **104** 1.
- [81] Wendong Wang et al. 2017 *Science Advances* **3** 5.
- [82] H. Pohl 1980 *The Quaterly Review of Biology* **55** 1.

- [83] Alice P. Gast and Charles F. Zukoski. 1989 *Advances in Colloid and Interface Science* **30**.
- [84] Richard W. OBrien and Lee R. White. 1978 *J. Chem. Soc. Faraday Trans. 2* **74**.
- [85] Seth Fraden, Alan J. Hurd, and Robert B. Meyer. 1989 *Phys. Rev. Lett.* **63** 21.
- [86] Frieder Mugele and Jean-Christophe Baret 2005 *Journal of Physics: Condensed Matter* **17** 28.
- [87] N. Aubry et al. 2008 *Proceedings of the National Academy of Sciences* **105** 10.
- [88] Lionel Foret and Alois Würger. 2004 *Phys. Rev. Lett.* **92** 5.
- [89] M. G. Nikolaides et al. 2002 *Nature* **420** 6913.
- [90] Nadine Aubry and Pushpendra Singh. 2008 *Phys. Rev. E* **77** 5.
- [91] N Aubry and P Singh. 2006 *Europhysics Letters* **74** 4.
- [92] Peter A. Kralchevsky and Nikolai D. Denkov. 2001 *Current Opinion in Colloid and Interface Science* **6** 4.
- [93] Bartosz A. Grzybowski et al. 2017 *Chem. Soc. Rev.* **46** 18.
- [94] Jérôme J Crassous et al. 2014 *Nature Communications* **5**.
- [95] J. Kadaksham, Praval Singh, and Nadine Aubry. 2006 *Mechanics Research Communications* **33**.
- [96] Sai Nudurupati et al. 2008 *ELECTROPHORESIS* **29** 5.
- [97] Kyuho Hwang, Pushpendra Singh, and Nadine Aubry. 2010 *ELECTROPHORESIS* **31** 5.
- [98] Sai Nudurupati et al. 2010 *Soft Matter* **6** 6.
- [99] Paul Dommersnes et al. 2013 *Nature Communications* **4**.
- [100] Geoffrey Ingram Taylor, A. D. McEwan, and L. N. J. de Jong. 1966 *Proceedings of the Royal Society of London. Series A. Mathematical and Physical Sciences* **291** 1425.
- [101] M. Janjua et al. 2009 *Mechanics Research Communications* **36** 1.
- [102] Alena Sergeeva, Dmitry Gorin, and Dmitry Volodkin. 2013 *BioNanoScience* **4**.

Figures

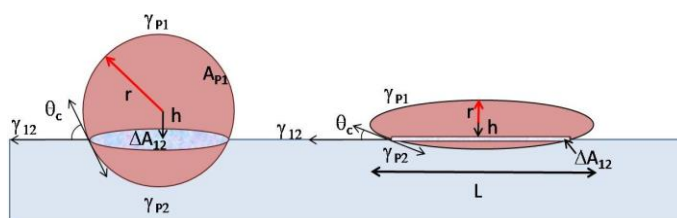


Figure 1: A sphere and ellipsoid at fluid-fluid interface. h is the height of the particle center of mass above the interface

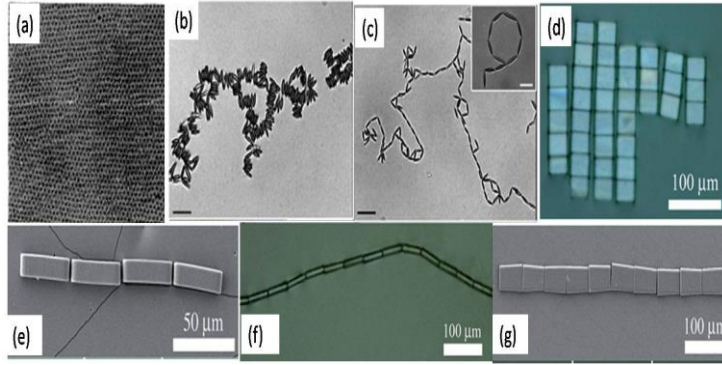


Figure 2: (a) 2D triangular lattice structure formed by polystyrene spheres at water/air interface [9]. Ellipsoidal particles are trapped at the water-oil interface. (b) Side to side aggregation (c) Tip-to-tip manner. Inset: Polygonal assembly formed by PS ellipsoids [37]. Assembly of particles having aspect ratio of (d) $a=2.0$ shows tiling, (e) $a=4.0$, (f) $a=0.2$ and (g) $a=0.6$ shows end-to-end chaining [21]

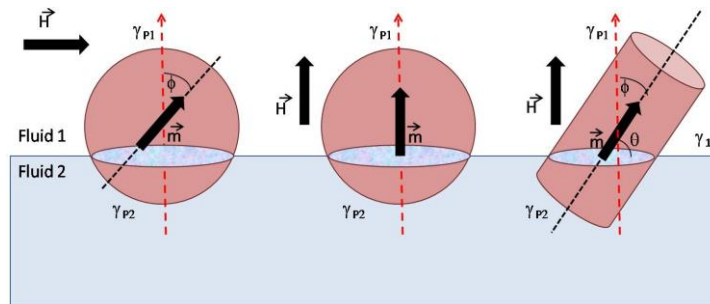


Figure 3: Spherical and cylindrical particles at fluid interfaces showing the relevant parameters

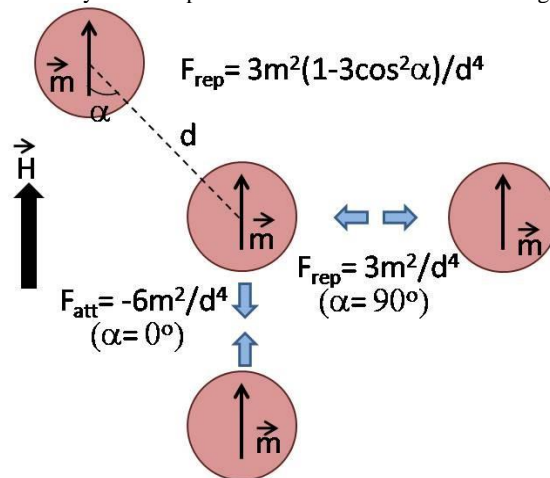


Figure 4: Interaction between particles in a magnetic field

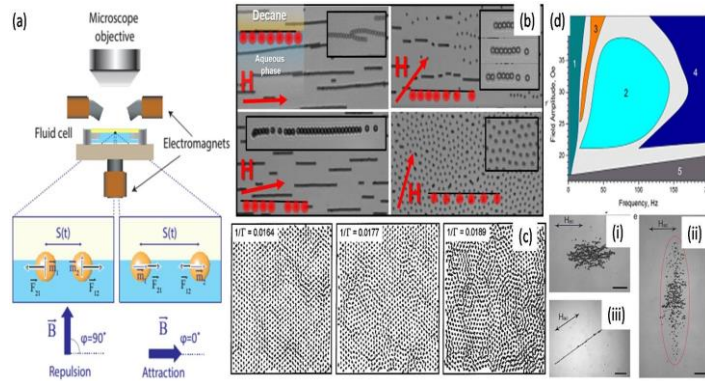


Figure 5: Magnetic field induced assembly of spheres at interfaces: (a) Principle of the Intra-Pair Magnetophoresis (IPM) experiment showing that pairs of particles are repelled and attracted by changing the orientation of the magnetic field generated by a set of electromagnets[63] (b) Chaining and disassembling of paramagnetic colloids at decane-water interface under varying magnetic field orientations.[54] (c) Trajectories of particles taken at three different temperatures corresponding to the solid phase(left) close to melting, the hexatic (middle), and the isotropic liquid phase(right)[53] (d) Dynamic self-assembled structures at the air-liquid interface under uniaxial alternating field parallel to the air-liquid interface. Phase diagram illustrating different states of magnetic dispersion versus the amplitude and frequency of the applied magnetic field. Region 1 depicts pulsating clusters (i). Region 2 corresponds to a gas of spinners (ii). Region 3 delineates phase boundaries of the perpendicular cloud phase. Region 4 corresponds to dynamic wires (iii). Particles form dense static clusters in Region 5.[72]

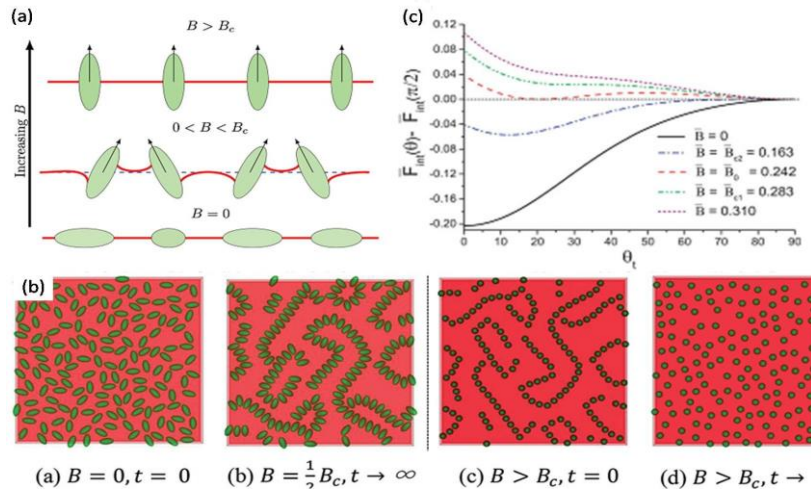


Figure 6: Magnetic field induced assembly of non-spherical particles at interfaces. (a) Orientation of ellipsoidal particles depicting flipping behaviour around critical field strength perpendicular to the interface. (b) Simulated top view of the ellipsoids around the critical strength showing formation of “capillary caterpillars”[86] (c) Variation of dimensionless free energy as a function of tilt angle for cylindrical particles for different field strengths[74]

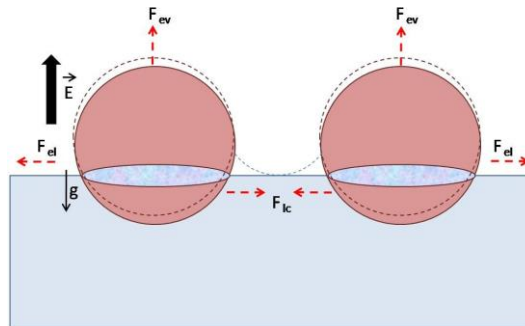


Figure 7: Various forces acting on a pair of spheres at interface under perpendicular electric field.

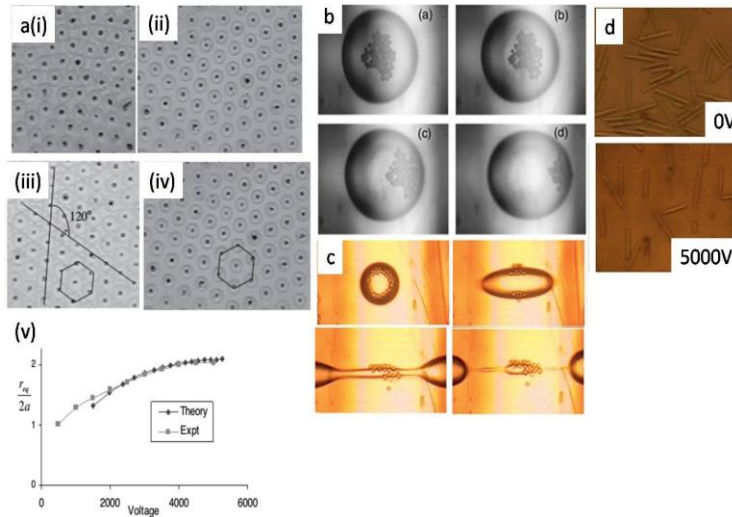


Figure 8: Interfacial assembly under electric field. (a) Assembly of glass particles floating at the air– oil interface under constant field (i) due to lateral capillary forces. The lattice is approximately triangular, but lacks long-range order and contains many defects. (ii) When a voltage of 5,000 volts is applied, particles move away from each other and form a defect-free triangular lattice (iii) The applied voltage is slowly decreased to 0 volts. Particles touch each other in a well organized triangular (hexagonal) lattice and the lattice exhibits long-range order that is indicated by the straight lines passing through their centers (iv) Monolayer for 3,500 volts. The lattice spacing is smaller than inband a hexagonal cell is shown. (v) Comparison of theory and experimental results of variation of equilibrium distance with volume [87, 91] (b) Movement of particles to equator on a water droplet in decane for the case of perpendicular AC field where DEP force is maximal. [96] (c) Removal of polystyrene spheres from a water drop immersed in corn oil. The voltage was continually increased and at an applied voltage of 1800 V at 100 Hz. Particles continued to move towards the equator while the drop quickly stretched with time (the sequence is shown in four photographs), and broke into three main droplets. The droplet in the middle contained all of the particles, and the larger sized droplets on the left and right sides were particle free. [98] (d) Rods at fluid interfaces experience electric force and torque and at high fields align end-to-end and the lattice spacing of a self-assembled monolayer of rods increases.[101]